Available online at www.sciencedirect.com

SciVerse ScienceDirect

Ceramics International 39 (2013) 5833–5843

CERAMICS INTERNATIONAL

www.elsevier.com/locate/ceramint

Preparation and photocatalytic properties of visible light-driven samarium-doped ZnO nanorods

Jin-Chung Sin, Sze-Mun Lam, Keat-Teong Lee, Abdul Rahman Mohamed*

School of Chemical Engineering, Universiti Sains Malaysia, Engineering Campus, 14300 Nibong Tebal, Pulau Pinang, Malaysia

Received 26 November 2012; received in revised form 22 December 2012; accepted 2 January 2013
Available online 16 January 2013

Abstract

Samarium-doped ZnO nanorods (Sm/ZNRs) were newly synthesized via a facile and surfactant-free solvothermal method. The as-synthesized products were characterized by X-ray diffraction (XRD), field emission scanning electron microscopy (FESEM) together with an energy dispersion X-ray spectrum (EDX) analysis, transmission electron microscopy (TEM), high resolution transmission electron microscopy (HRTEM), UV–visible diffuse reflectance spectra (UV–vis DRS) and photoluminescence (PL) spectra. The XRD and EDX results revealed that Sm ion was successfully doped into ZNRs. It was also observed that the Sm doping increased the visible light absorption ability of Sm/ZNRs and a red shift for Sm/ZNRs appeared when compared to pure ZNRs. The photocatalytic activity of the products was evaluated by the photocatalytic degradation of phenol aqueous solution under visible light irradiation. The results showed that all the Sm/ZNRs exhibited higher photocatalytic activities than that of the pure ZNRs. Such enhancement was attributed to their high charge separation efficiency and •OH generation ability as evidenced by the PL spectra. The photocatalytic studies also showed that various effects of parameter had remarkable effect on the degradation rate of phenol. In addition, the one-dimensional structure of Sm/ZNRs could be easily recycled and reused, showing great potential for practical applications in environmental cleanup.
© 2013 Elsevier Ltd and Techna Group S.r.l. All rights reserved.

Keywords: A. Powders: chemical preparation; C. Optical properties; D. ZnO

1. Introduction

ZnO, as a potential semiconductor with direct wide band gap (~3.3 eV), has received enormous scientific attention due to its excellent electrical optoelectronic properties and wide potential applications in piezoelectric nano-generators, dye-sensitized solar cells, chemical sensors and photocatalysts for degradation and complete elimination of environmental pollutants [1–3]. It has been demonstrated that physical and chemical properties are generally determined by the morphology and dimensionality in micro- and nano-scale systems. Hitherto, there have already been many approaches for the synthesis of ZnO with different morphologies and structures, including nanorods, nanowires, nanobelts, nanosheets, nanoflowers, cuboid shaped, hierarchical and complex ZnO micro-architectures [4–11]. These approaches can be classified into the solvothermal method, the thermal evaporation process, the sol–gel method, the electrochemical deposition technique and the sonochemical route [4,6,7,10,11].

Solvothermal method is one of the promising methods to prepare ZnO, because it is an environmental friendly soft solution chemical route to reach hardy target by inducing complicated reactions, which may not take place in normal conditions, under the huge self-produced pressure by sub- or supercritical solvents [12]. Based on this method, various morphologies of ZnO have been synthesized by introducing different solvents [4,13,14]. In particular, one-dimensional (1D) ZnO nanorods have high surface area and good dispersibility in solution rate, which enable them to act as promising photocatalysts for photocatalytic degradation of water pollutants [15]. Also our group has recently shown that ZnO nanorods can improve the photocatalytic activity for endocrine disrupting chemicals degradation [16]. However, the low quantum yields and the lack of visible-light utilization forestalled this technique in the practical application. To address this lapse, modifications of ZnO nanostructures including

*Corresponding author. Tel.: +60 45996410; fax: +60 45941013.
E-mail address: chrahman@eng.usm.my (A.R. Mohamed).

0272-8842/$ - see front matter © 2013 Elsevier Ltd and Techna Group S.r.l. All rights reserved.
http://dx.doi.org/10.1016/j.ceramint.2013.01.004

doping of metal or non-metal ions, deposition of noble metals as well as use of coupled semiconductors have been proposed [16–18]. Recently, some studies have reported doping with rare earth ions was a useful way for improving the above two performances of ZnO [18,19]. The doping of rare earth ions on the ZnO produced impurity energy levels in band gap and expanded its visible light response; furthermore, it produced traps for photogenerated charge carriers, thus accelerating the interfacial charge transfer and inhibiting the recombination of electron–hole pairs [19]. Although some rare earth metal ions have been used as dopants to modify ZnO, to the best of our knowledge, the application of Sm^{3+}-doped ZnO nanorod as a photocatalyst has not been reported yet.

On the basis of the above consideration, this work reports for the first time on the synthesis of Sm-doped ZnO nanorods (Sm/ZNRs) via a facile and surfactant-free solvothermal method as photocatalysts. A possible explanation of the formation of the nanorod structure was presented. The as-synthesized ZnO products were characterized by different techniques and used for the photocatalytic degradation of phenol under visible light irradiation. The effects of Sm doping content in Sm/ZNRs, catalyst amount, initial substrate concentration as well as solution pH on the photocatalytic activities of Sm/ZNRs were investigated. Moreover, the stability of as-synthesized Sm/ZNRs was studied through successive three cycles of experiments. The mechanisms of influence on the photocatalytic activity of the Sm/ZNRs were also discussed.

2. Experimental details

2.1. Preparation of Sm/ZNRs

All the reagents used in this work were of analytical grade without further purification. The detailed synthesis procedure was as follows: 4.0 mmol zinc acetate dihydrate ($Zn(CH_3COO)_2 \cdot 2H_2O$) and samarium (III) nitrate hexahydrate ($Sm(NO_3)_3 \cdot 6H_2O$) with different Sm/Zn ratios (0, 0.5, 1.0 and 2.0 at%) were dissolved into 60 ml ethanol under vigorous stirring for 3 h. At the same time, 60 mmol NaOH was dissolved into 100 mL ethanol and a homogeneous solution was obtained after constant stirring for 3 h. Then the solution containing $Zn(CH_3COO)_2 \cdot 2H_2O$ and $Sm(NO_3)_3 \cdot 6H_2O$ was added drop-wise into the alkaline solution under stirring. After being stirred for 1 h, the resulting solution was transferred to a 200 mL Teflon-sealed autoclave and maintained at a temperature of 150 °C for 20 h and then allowed to cool to room temperature naturally. The as-formed precipitates were filtrated, washed with deionized water and ethanol for several times, dried at 60 °C in air for 12 h and finally calcined at 450 °C in air for 2 h.

2.2. Characterization

The products were characterized by X-ray diffraction (XRD) analysis on a Philip PW1820 diffractometer equipped with Cu Kα radiation over a range from 20° to 80°. The field emission scanning electron microscopy (FESEM) analysis was carried out using a Quanta FEG 450 together with an energy dispersion X-ray spectrum (EDX) analysis. Transmission electron microscopy (TEM) image was taken on a Philip CM 12 instrument operating at 120 keV. High resolution TEM (HRTEM) image was performed on a Tecnai 20 at 200 keV. The diffuse reflectance spectroscopy (DRS) of catalysts was tested in a Perkin Elmer Lambda 35 UV–vis spectrometer. The spectra were recorded timely in the range of 300–600 nm using $BaSO_4$ as the reference standard. Photoluminescence (PL) spectroscopy of synthesized products was taken at room temperature on a Perkin Elmer Lambda S55 spectrofluorometer using a Xe lamp with an excitation wavelength of 325 nm.

2.3. Measurement of photocatalytic activity

The photocatalytic activity of the as-synthesized ZnO products was evaluated by the degradation of phenol in water. Experiment was as follows: 100 mg catalyst was placed into 100 mL of phenol aqueous solution (20 mg/L) in a beaker. A 55 W compact fluorescent lamp was used as the light source to provide visible light irradiation. It was placed above the beaker at a distance of 12 cm. The average light intensity striking the surface of the reaction solution was about 14500 Lux, as measured by a digital luxmeter. Before photocatalytic reaction, the solution was magnetically stirred in dark for 1 h to ensure the establishment of an adsorption–desorption equilibrium between the catalyst and phenol. The phenol concentration after equilibration was monitored using a high-performance liquid chromatography (HPLC) and taken as the initial concentration (C_o). The details of the photocatalytic process and HPLC system have already been discussed in our earlier papers [16,20]. The reaction temperature was kept at room temperature by using cooling fans to prevent any thermal catalytic effect. After the elapse of a period of time, 2 mL of the solution was drawn and the concentration of phenol (C) was determined. The dissolution of ZnO in the course of photoreaction was estimated on a Shimadzu AA-6650 atomic absorption spectrophotometer (AAS). Standard solutions bracketing the Zn^{2+} content of samples were prepared and ran at the same time as the test samples.

The durability test of the as-synthesized ZnO products was also performed by using the same procedure as above and the product underwent three consecutive cycles, each lasting for 480 min. After each cycle, the catalyst was centrifuged and washed thoroughly with deionized water, and then added to fresh phenol solution. In order to determine the reproducibility of all the results, at least duplicated runs were carried out for each condition for averaging the results, and the experimental error was found to be within $\pm 4\%$.

2.4. Analysis of hydroxyl radicals (•OH)

The formation of hydroxyl radicals (•OH) on the surface of photo-illuminated ZnO products was detected by the PL technique using terephthalic acid as a probe molecule. Terephthalic acid readily reacted with •OH to produce highly fluorescent product, 2-hydroxyterephthalic acid. This technique has been used in radiation chemistry, sonochemistry, and biochemistry for the detection of •OH generated in water [21]. The method relied on the PL signal at 425 nm of 2-hydroxyterephthalic acid. The PL intensity of 2-hydroxyterephthalic acid was proportional to the amount of •OH formed. Experimental procedures were similar to those used in the measurement of photocatalytic activity except the aqueous solution of phenol was replaced by the 5×10^{-4} M terephthalic acid with a concentration of 2×10^{-3} M NaOH solution. The PL spectra of generated 2-hydroxyterephthalic acid were measured by a Perkin Elmer Lambda S55 spectrofluorometer. At the intervals of given irradiation time, the reaction solution was used to measure the increase of the PL intensity at 425 nm by excitation with a wavelength of 315 nm.

3. Results and discussion

3.1. Characterization of the as-synthesized products

Fig. 1 is the XRD patterns of as-synthesized products. The diffraction peaks in the XRD spectra indicated that all the products had typical hexagonal wurtzite structures. For Sm/ZNRs, no diffraction peaks of Sm or other impurity phases were detected, suggesting that Sm^{3+} ions would uniformly substitute into the Zn^{2+} sites in the lattices of ZNRs. In addition, the diffraction peaks of ZNRs became broader in width and weaker in intensity with increase in the nominal content of Sm, inferring that Sm doping inhibited the growth of crystal size. It was also

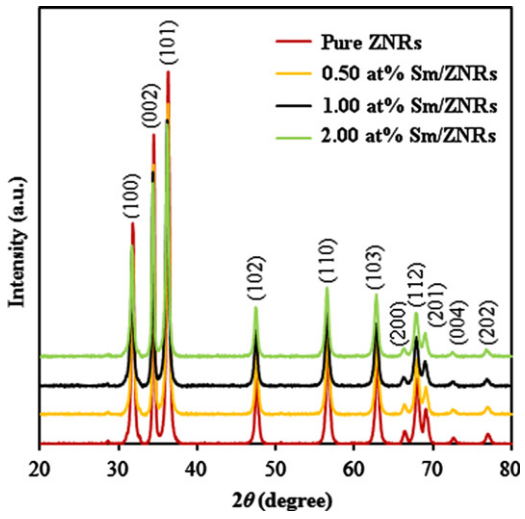

Fig. 1. XRD patterns of pure ZNRs and Sm/ZNRs with different doping contents of Sm.

reported that rare earth ions (i.e. La^{3+}, Nd^{3+} and Er^{3+}) doping restrained the increase of crystals of ZnO [22–24]. The decrease in the crystal size of Sm/ZNRs was mainly attributed to the formation of Sm–O–Zn on the surface of the doped products, which inhibited the growth of crystal grains [22].

Fig. 2 shows the FESEM images of pure ZNRs and 1 at% Sm/ZNRs. It can be seen that the synthesized products were rod shaped and grown in large quantity. The nanorods were 68–139 nm diameter and 1–3 μm long for pure ZNRs (Fig. 2(a) and (c)). Upon doping with Sm in Fig. 2(b) and (d), the diameter of 1 at% Sm/ZNRs became 43–103 nm. The average diameter of the as-synthesized Sm/ZNRs was smaller than that of the pure ZNRs. Furthermore, the growth of ZNRs was not influenced by the doping of Sm atoms as the $Sm(NO_3)_3\cdot6H_2O$ was used for providing Sm^{3+} ions to be doped, and the molar content of the dopant agent in comparison with ZnO source was too small to alter the morphology. Fig. 2(e) is an EDX pattern of the 1 at% Sm/ZNRs indicating the products were made up of Zn, O and Sm ions which showed that the Sm dopant was successfully incorporated into the ZnO. The average of Sm/Zn atomic ratio was derived to be about 0.0091, which was close to the experimental dopant concentration.

For detailed microstructure characteristics of the Sm/ZNRs, TEM along with HRTEM analyses were done and results are indicated in Fig. 3. Fig. 3(a) exhibits the typical TEM image of 1 at% Sm/ZNRs. It was clearly demonstrated that the product revealing rod-shaped morphology, which can coincide with the obtained FESEM investigations. The HRTEM image in Fig. 3(b) showed that the interplanar spacing of the nanorod was 0.26 nm corresponding to the *d*-spacing of (002) plane of ZnO, which indicated that the nanorod grew along the [0001] direction. From the TEM and HRTEM images, it can be verified that the synthesized products have highly crystalline structure, which was essential for excellent photocatalytic materials.

Fig. 4 shows the UV–vis DRS spectra of all the Sm/ZNRs products along with the pure ZNRs. Modification of ZNRs with samarium significantly affected the light absorption property of the photocatalysts. It was noticeable that the light absorption of Sm/ZNRs in the visible light range (>400 nm) was higher than that of pure ZNRs and the light absorption increased with increasing Sm content. Furthermore, a slight red shift of the optical absorption edge was observed for all the doped products compared to pure ZNRs. The observed red shift indicated the narrower band gap originated from the charge transfer between the ZnO valence or conduction band and the Sm ion 4f level [25]. The band gap energies of the products were calculated according to Eq. (1) [23]:

$$E_g = hc/\lambda = 1240/\lambda \quad (1)$$

where E_g is the band gap energy (eV), h is the Planck's constant (4.135667×10^{-15} eVs), c is the velocity of light (3×10^{8} m/s), and λ is the wavelength (nm) of absorption

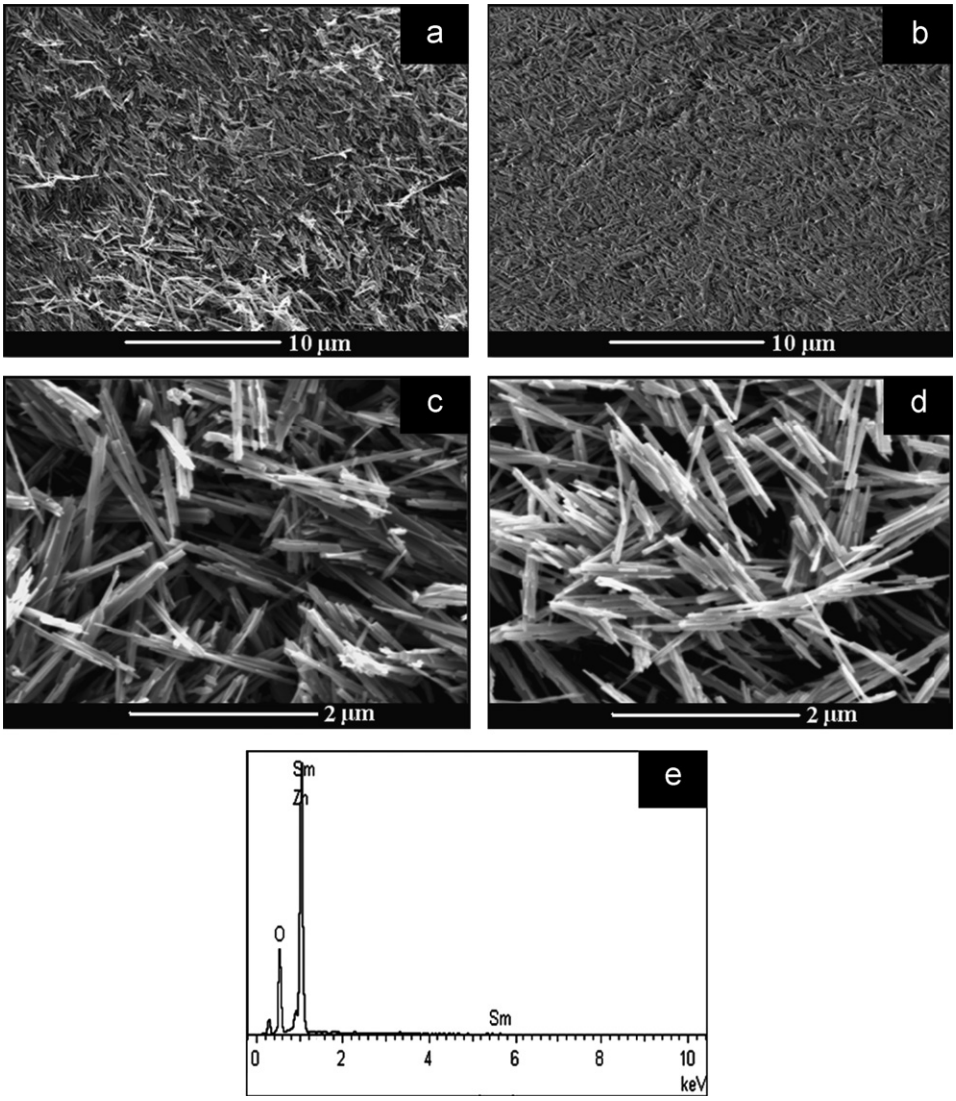

Fig. 2. (a),(c) FESEM images of pure ZNRs; (b),(d) FESEM images of 1 at% Sm/ZNRs; (e) The EDX spectrum of 1 at% Sm/ZNRs.

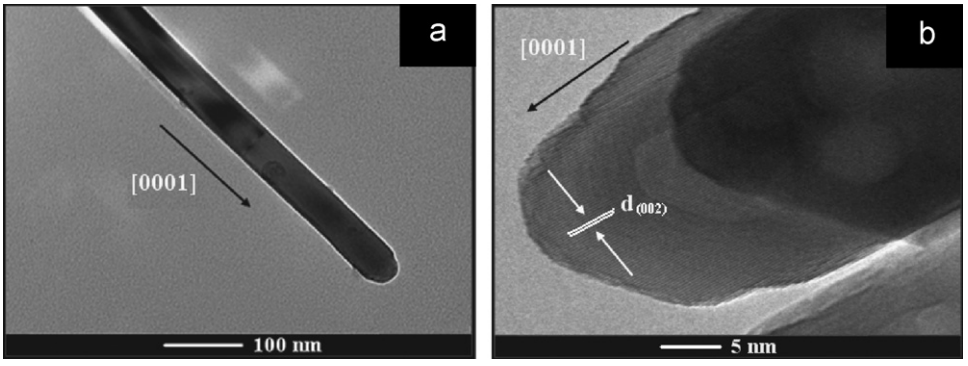

Fig. 3. (a) TEM image and (b) HRTEM image of 1 at% Sm/ZNRs.

onset. Using Eq. (1), the measured band gap energies of the 0.5 at% Sm/ZNRs, 1 at% Sm/ZNRs and 2 at% Sm/ZNRs were 3.25, 3.24, 3.23 eV, respectively, lower than that of pure ZNRs (3.27 eV). Above results revealed that the Sm/ZNRs can absorb in UV as well as in visible region of the solar light. Hence, the absorption property deduced that the Sm/ZNRs could be promising in visible light photocatalysis.

3.2. Possible growth mechanism of nanorod-like ZnO structure

On the basis of studies mentioned above, the growth of ZnO could be proposed based on the chemical reactions involved and crystal growth habits of ZnO. The reaction process can be expressed as follows:

$$Zn^{2+} + 4OH^- \rightarrow Zn(OH)_2\downarrow$$

$$Zn(OH)_2 + 4OH^- \rightarrow Zn(OH)_4^{2-}$$

$$Zn(OH)_4^{2-} \rightarrow ZnO + H_2O + 4OH^-$$

The reaction (2) could be easily observed when adding NaOH to the Zn^{2+} solution. As more of the NaOH solution was added, the $Zn(OH)_2$ precipitate dissolved to yield a homogenous aqueous solution containing $Zn(OH)_4^{2-}$ ions. Upon increasing the time further, ZnO nuclei formed from the dehydration of $Zn(OH)_4^{2-}$ ions and followed by crystal growth.

Generally, ZnO crystallites with the hexagonal wurtzite structure are polar as the Zn and O ions combine together through tetrahedral coordination, leading to the polar symmetry along the hexagonal axis. It is well recognized that there are two polar planes for ZnO crystallites: one is the positive polar plane terminated by Zn (0001) and another is the negative polar plane terminated by O ($000\bar{1}$). The Zn-terminated ZnO plane is catalytically active while the O-terminated plane is inert [26]. Moreover, the growth habit depends upon the growth velocities of different planes in the ZnO crystal. Laudise and Ballman reported that the higher the growth rate, the faster the disappearance of a plane, which led to the pointed shape on the end of the *c*-axis [27]. In ZnO, the growth velocities of the ZnO plane in different directions were $[0001] > [01\bar{1}\bar{1}] > [01\bar{1}0] > [01\bar{1}1] > [000\bar{1}]$ [27]. Thus, the ZnO crystallites grow very fast along [0001] direction (*c*-axis), which leads to the formation of nanorod-like structure. In our work, the ZnO nanorod was synthesized without the use of any surfactant, and it is also a facile way for large-scale synthesis of 1D ZnO structures.

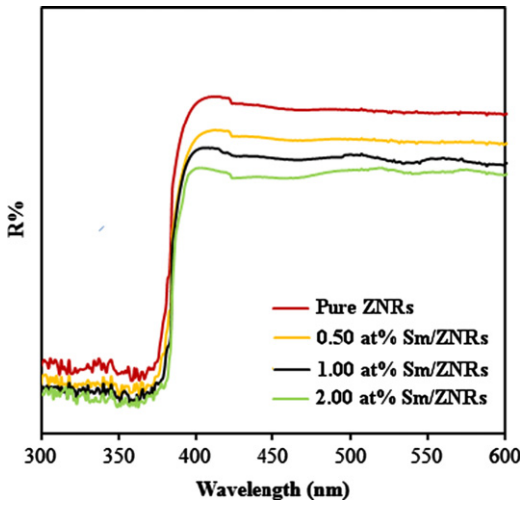

Fig. 4. UV–vis DRS spectra of pure ZNRs and Sm/ZNRs with different doping contents of Sm.

3.3. Photocatalytic activity

The photocatalytic activities of the as-synthesized ZnO products were evaluated by the degradation of phenol aqueous solution. Phenol is an endocrine disrupting chemical which produced worldwide in millions of tons each year and widely used in manufacturing of resins, insulation panels, pesticides, paints and lubricants. The extensive use and poor biodegradability of phenol have resulted in its ubiquitous presence in the environment and have led to contamination of surface and ground waters [28]. Evidence of phenol effect came from observation of increased chromosome aberrations in spermatogonia and primary spermatocytes of mice treated with a solution of

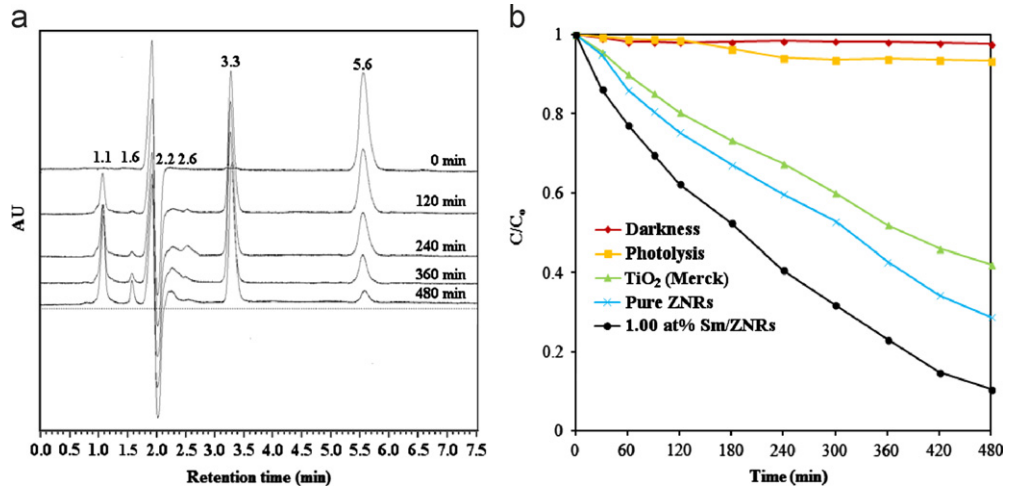

Fig. 5. (a) Time-dependent HPLC chromatogram of phenol aqueous solution over the 1 at% Sm/ZNRs ([phenol]=20 mg/L; catalyst amount=1.0 g/L; pH=5.2). (b) Phenol concentration dependence on irradiation time using various photocatalysts ([phenol]=20 mg/L; catalyst amount=1.0 g/L; pH=5.2).

phenol in water [29]. Thus, phenol was chosen as the model substrate to evaluate the photocatalytic activities of the as-synthesized ZnO products in this work. The HPLC profiles during the photodegradation of phenol over the 1 at% Sm/ZNRs are shown in Fig. 5(a). The phenol showed a characteristic peak at retention time (RT) 5.6 min; it became weaker with the extended irradiation time and nearly disappeared after 480 min, indicating the excellent photocatalytic activity of the product. In addition to the above-mentioned main compound, the peaks at RT 1.1 min, 1.6 min, 2.2 min, 2.6 min and 3.3 min could be assigned to muconic acid, pyrogallol, hydroquinone, resorcinol and benzoquinone intermediates, respectively when compared with the standard chemicals. This identification was also consistent with that reported in other studies [30–32]. The proposed photodegradation pathways are shown in Scheme 1, where hydroquinone, resorcinol and pyrogallol would be generated as by-products in the initial stage of the degradation [32]. It should also be noted that benzoquinone would be generated due to dehydrogenation reaction of hydroquinone [33]. These aromatic intermediates would undergo ring cleavage reaction to yield aliphatic acids such as muconic acid, which would eventually convert to CO_2 and H_2O due to decarboxylation [31].

Fig. 5(b) shows that the degradation efficiency of 1 at% Sm/ZNRs reached 89.5% in 480 min. Under identical experimental conditions, the 1 at% Sm/ZNRs showed much higher activities than pure ZNRs (71.2% degradation efficiency) and commercial TiO_2 (58.9% degradation efficiency). Further comparative experiments were also performed to evaluate the catalytic activity. As can be seen, the phenol concentration decreased by less than 6.7% after 480 min irradiation in the absence of catalysts, inferring no obvious photolysis. With 1 at% Sm/ZNRs alone without exposure to light irradiation, loss of phenol in solution was not evident, showing insignificant adsorption of phenol onto the catalysts. These results also revealed that the photocatalytic reactions were induced by the catalyst in combination with light irradiation which led to degradation of phenol aqueous solution.

The photocatalytic degradation of phenol obeyed the pseudo-first-order kinetics. At low initial phenol concentration the rate expression is given by:

$$d[\mathrm{C}]/dt = k[\mathrm{C}] \tag{5}$$

where k is the observed rate constant. The phenol was adsorbed onto the catalyst surface and the adsorption–desorption equilibrium was reached in 1 h. After adsorption, the equilibrium concentration of phenol was determined and considered as the initial phenol concentration for kinetic analysis. On integrating the above equation, Eq. (6) was obtained.

$$\ln(C_o/C) = kt \tag{6}$$

where C_o is the equilibrium concentration of phenol and C is the concentration at time t.

3.3.1. Effect of Sm doping content

The degradation of phenol in the presence of Sm/ZNRs with different Sm doping contents was measured and the results are shown in Fig. 6. As can be seen, all the products of Sm/ZNRs demonstrated higher photocatalytic activities than that of pure ZNRs. Especially, Sm/ZNRs with a Sm content of 1 at% exhibited the best performance on the photodegradation of phenol among the four products. At low Sm content (≤ 1 at%), the photocatalytic activities of the Sm/ZNRs increased gradually with an increase of the Sm content ($1.0 > 0.5 > 0$ at%). However, with increasing Sm content to 2 at%, the photocatalytic activities of the products decreased. According to kinetic analysis, the k values are calculated and shown in Table 1. The results clearly demonstrated that the k value

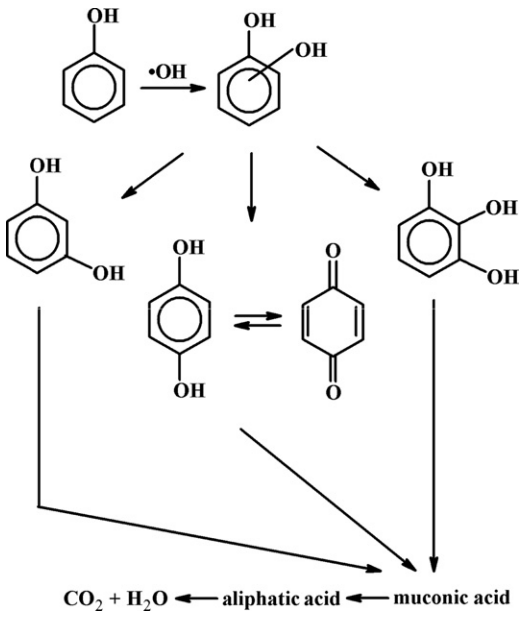

Scheme 1. Proposed reaction pathway for photodegradation of aqueous phenol by the Sm/ZNRs products.

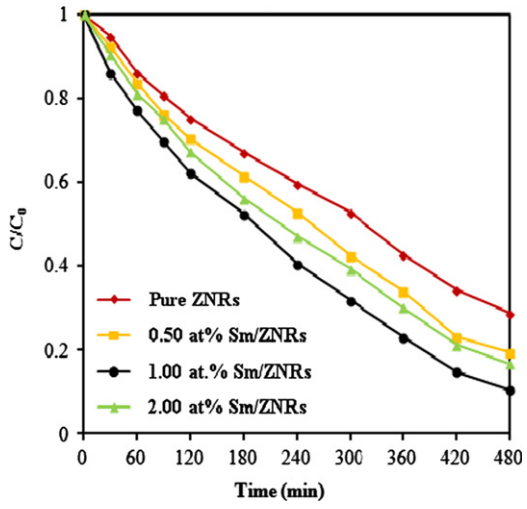

Fig. 6. Effect of Sm doping content in Sm/ZNRs on phenol degradation ([phenol]=20 mg/L; catalyst amount=1.0 g/L; pH=5.2).

of 1 at% Sm/ZNRs reached the highest and was about two times that of pure ZNRs. The k value of 2 at% Sm/ZNRs was lower than that of 1 at% Sm/ZNRs, which further revealing that the enhanced activity of the photocatalysts does not increase further for more Sm doping. As for enhancement of the photocatalytic activity of the Sm/ZNRs, it will be discussed in detail below.

3.3.2. Effect of Sm/ZNRs amount

Photocatalyst amount is one of the priority variables to the degradation efficiency of organic pollutants. The effect of 1 at% Sm/ZNRs amount was studied over a range of 0.5–3.0 g/L, and the corresponding k value of phenol degradation is shown in Table 1. The degradation efficiency of phenol enhanced with increase in catalyst amount up to 2.0 g/L owing to the increasing presence of catalyst sites. Above 2.0 g/L 1 at% Sm/ZNRs a decrease in degradation efficiency was observed which could be due to the reduction in the penetration of light and light scattering by excess catalyst [34].

3.3.3. Effect of initial substrate concentration

The dependency of photocatalytic degradation of phenol on the initial substrate concentration was investigated in the presence of 2.0 g/L 1 at% Sm/ZNRs. Table 1 shows that the k value of phenol degradation decreased from 0.0057 to 0.0028 min^{-1} with increase in the initial phenol concentration from 20 to 60 mg/L. The rate of degradation is related to the active species formation on catalyst surface and probability of active species reacting with phenol molecules. For all initial phenol concentrations, the catalyst amount and irradiation time were constant. Since the generation of active species remained the same, the probability of phenol molecule to react with the active species decreased. The increase in phenol concentration also decreased the path length of photon entering into the phenol solution and this may reduce the degradation efficiency.

3.3.4. Effect of solution pH

The effect of solution pH on photocatalytic degradation of phenol was studied in the pH range of 3.0–10.0 and the corresponding results are shown in Table 1. The pH of the solution was adjusted by adding small amount of equimolar HCl or NaOH before irradiation. The range covered the pH at point of zero charge (pzc) of ZnO and pKa of phenol which were 9.3 and 9.9, respectively [3]. It was observed that increase in pH from 3.0 to 5.2 (natural pH) increased the degradation efficiency of phenol and then decreased. The interpretation of pH effects on the efficiency of phenol photodegradation process is a very intricate task because of its multiple roles. First, dissociation ions from pH adjustors could create competition with the phenol molecules on the surface of ZnO. It was noted that in acidic condition, Cl^- ions from HCl might have been adsorbed on the surface of ZnO and decreased the phenol degradation [35,36]. On the other hand, in alkaline condition, the pH was adjusted by NaOH. The competitive adsorption of the ions from NaOH salt might also result in lower photocatalytic activity [36]. Moreover, at higher pH, the surface of ZnO was negatively charged and phenolate anions can be repelled away from the ZnO surface which opposed degradation of substrate molecules on the surface of photocatalyst. For pH 5.2, however, the Cl^- ions did not exist because the natural pH did not require the addition of any HCl to adjust the pH solution. Thus, the electrostatic attraction between positively charged ZnO with molecular form of phenol molecules led to a maximum degradation efficiency of phenol.

Next, was related to the dissolution of ZnO under highly acidic or highly alkaline conditions according to the following reactions:

$$ZnO + 2H^+ \rightarrow Zn^{2+} + H_2O \text{ (acidic dissolution)} \quad (7)$$

$$ZnO + H_2O + 2OH^- \rightarrow Zn(OH)_4^{2-} \text{ (alkaline dissolution)} \quad (8)$$

In a strongly acidic environment, ZnO dissolved readily to yield Zn^{2+} ions, while under alkaline environment ZnO underwent dissolution into $Zn(OH)_4^{2-}$ [37–39]. This explained the decrease in the rate of photodegradation under highly acidic or alkaline conditions. Taking into account the aforementioned reasons, the optimum solution pH was 5.2, which was the natural value of the aqueous phenol solution. The ZnO dissolution data at pH 5.2 collected from AAS revealed the loss of ZnO was mostly low or negligible ($< 0.04\%$) and did not increase appreciably with irradiation time.

Table 1
Effects of Sm doping content, catalyst amount, initial phenol concentration and solution pH on the photocatalytic activities of Sm/ZNRs.

Sm content (at%)[a]	k (min^{-1})	Catalyst amount (g/L)[b]	k (min^{-1})	Initial phenol concentration (mg/L)[c]	k (min^{-1})	Solution pH[d]	k (min^{-1})
0	0.0024	0.5	0.0039	20	0.0057	3.0	0.0033
0.50	0.0032	1.0	0.0043	40	0.0036	5.2	0.0057
1.00	0.0043	2.0	0.0057	60	0.0028	7.0	0.0039
2.00	0.0035	3.0	0.0050			10.0	0.0016

[a] [phenol] = 20 mg/L, catalyst amount = 1.0 g/L and pH = 5.2.
[b] 1 at% Sm/ZNRs, [phenol] = 20 mg/L and pH = 5.2.
[c] 1 at% Sm/ZNRs, catalyst amount = 2.0 g/L and pH = 5.2.
[d] 1 at% Sm/ZNRs, [phenol] = 20 mg/L and catalyst amount = 2.0 g/L.

In summary, the highest k value of phenol degradation can be obtained by controlling the influencing factors such as Sm doping content (1 at%), Sm/ZNRs amount (2.0 g/L), initial phenol concentration (20 mg/L) and solution pH (pH 5.2).

3.3.5. Reusability of the catalyst

Cycling uses as well as maintaining high photocatalytic activity are critical issues for long-term use in practical applications of the catalyst. Therefore, two criteria are required to be considered: (i) the stability of the catalyst to maintain its high activity over time. As shown in Fig. 7(a), after a three-time recycling of 1 at% Sm/ZNRs, there was still considerable degradation of phenol in the aqueous solution. Fig. 7(b) shows the XRD pattern of 1 at% Sm/ZNRs after the third catalytic reaction. It can be observed that the crystallization was still well maintained after recycling test, which illustrated that the photocatalyst was stable. (ii) The ease with which the catalyst could be recycled from solution. In this study, the products were of 1D nanorod morphology and could be easily separated from the aqueous suspensions by sedimentation, probably due to the large length to diameter ratio of the 1D Sm/ZNRs. It was indicated that the 1 at% Sm/ZNRs showed efficient photocatalytic activity for the degradation of organic pollutants under visible light irradiation and could easily be recycled for reuse.

3.4. Mechanism of phenol photodegradation

3.4.1. Photoluminescence emission spectra

PL spectrum is a useful tool to investigate the fate of photogenerated electron and hole in a semiconductor, since PL emission results from the recombination of free charge carriers. Generally, a weaker PL intensity implies a low recombination rate of the electron–hole under light irradiation [40]. Fig. 8 shows the PL spectra of Sm/ZNRs with different contents of Sm when the excitation wavelength was 325 nm. It can be observed that the pure ZNRs have the highest PL intensity, while the 1 at% Sm/ZNRs have the lowest PL intensity. Such PL results were consistent with the photocatalytic activity of the products. According to Pleskov [41], the value of the space charge region potential for an efficient separation of the photogenerated charge carriers had a lower limit. As the doping content of Sm increased (<1 at%), the surface barrier became higher and the space charge region became narrower. The electron–hole pairs within the region were thus efficiently separated by the large electric field before recombination which led to the lower PL intensity and caused an increase in the photocatalytic activity. Nevertheless, when the doping content was high (>1 at%), the space charge layer became very narrow and the penetration depth of light into ZnO greatly exceeded the space charge layer; therefore the recombination of the photogenerated electron–hole pairs became easier, which increased the PL intensity and retarded the photocatalytic activity of ZnO for phenol degradation.

3.4.2. Hydroxyl radical analysis

Fig. 9 shows the PL spectral changes observed after each product was irradiated for 240 min of visible light in the aqueous basic solution of terephthalic acid. An obvious difference in PL intensity at about 425 nm was observed using different catalysts. It was clear that the formation rate of •OH on the 1 at% Sm/ZNRs was higher than that of other products. This implied that the former has higher photocatalytic activity than the latter, which was also consistent with the results of PL emission spectra in Fig. 8. Moreover, all the Sm/ZNRs exhibited higher PL intensity than pure ZNRs, suggesting that doping of Sm on ZNRs was a good route to accelerate the interfacial charge transfer and inhibit the recombination of electron–hole pairs, which resulted in the increase of •OH formation.

Moreover, the inset of Fig. 9 depicts the change of PL spectra with irradiation time for the case of 1 at% Sm/

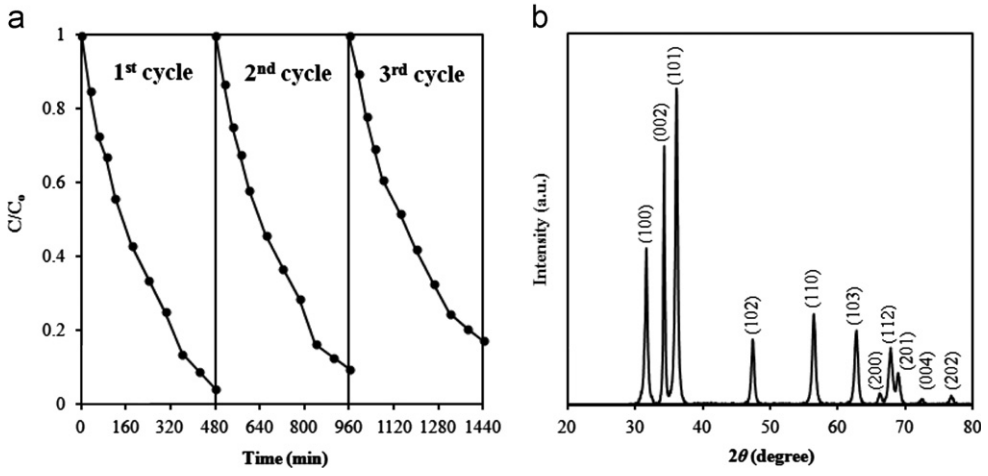

Fig. 7. (a) Cycling degradation curve for 1 at% Sm/ZNRs ([phenol]=20 mg/L; catalyst amount=2.0 g/L; pH=5.2). (b) XRD pattern of 1 at% Sm/ZNRs after the third cycling degradation experiment.

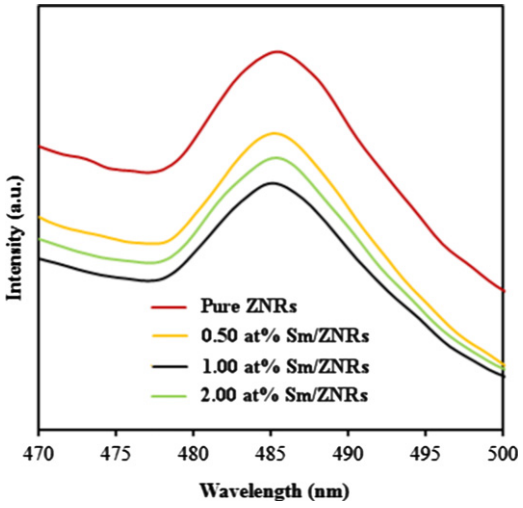

Fig. 8. PL spectra of pure ZNRs and Sm/ZNRs with different doping contents of Sm.

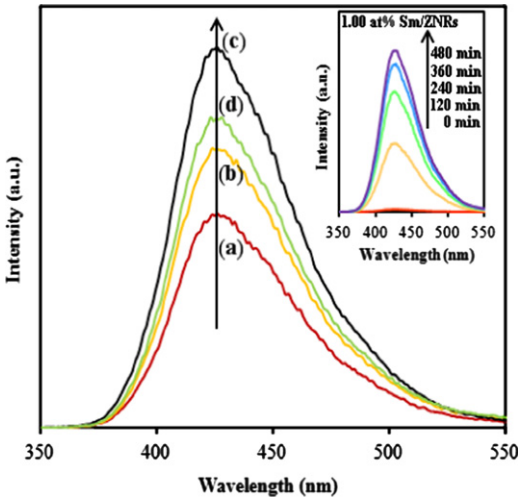

Fig. 9. PL spectra of the aqueous basic solution of terephthalic acid with an excitation at 315 nm under different products (a) pure ZNRs, (b) 0.50 at% Sm/ZNRs, (c) 1.00 at% Sm/ZNRs and (d) 2.00 at% Sm/ZNRs for 240 min. Inset is the PL spectra changing with irradiation time for the case of 1.00 at% Sm/ZNRs.

ZNRs. A gradual increase in PL intensity was observed with increasing irradiation time, which suggested that the fluorescence was caused by chemical reactions of terephthalic acid with •OH formed during photoilluminated reactions. Thus, these results further confirmed the evidence of •OH formation and indeed participated in degradation process.

Combining our experiment results with the related literatures [3,34,42], a postulated mechanism for the enhanced photocatalysis of Sm/ZNRs could be proposed in Scheme 2. Under the irradiation, the electrons (e_{cb}^-) are excited from the valence band to the conduction band of ZNRs leaving behind positively charged holes (h_{vb}^+). Sm^{3+} doping in ZNRs being strong Lewis acid due to the presence of partially filled f-orbital can effectively trap the e_{cb}^- and inhibit the recombination with h_{vb}^+. The reduced state of Sm^{2+} ions, with 6f electrons, are very instable so that the e_{cb}^- can be easily detrapped and transferred to the O_2 molecules promoting the superoxide anion radicals ($O_2{\bullet}^-$) formation and then converted to active •OH. This suggested that the Sm dopant can serve as an effective charge carrier trap and facilitated the excited e_{cb}^- transfer under visible light irradiation. The degradation mechanism for the Sm/ZNRs can be given as [42]:

$$ZnO + h\nu \rightarrow ZnO(e_{cb}^- + h_{vb}^+) \quad (9)$$

$$Sm^{3+} + e_{cb}^- \rightarrow Sm^{2+} \text{ (electron trapping)} \quad (10)$$

$$Sm^{2+} + O_2 \rightarrow Sm^{3+} + O_2{\bullet}^- \text{ (electron transfer)} \quad (11)$$

$$O_2{\bullet}^- + H^+ \rightarrow {\bullet}OOH \quad (12)$$

$${\bullet}OOH + H^+ + e_{cb}^- \rightarrow H_2O_2 \quad (13)$$

$$H_2O_2 + e_{cb}^- \rightarrow {\bullet}OH + OH^- \quad (14)$$

At the same time, the photogenerated h_{vb}^+ can trap on the catalyst surface undergoing charge transfer with adsorbed water molecules or with surface-bound hydroxide species to generate active •OH as shown in steps:

$$h_{vb}^+ + H_2O \rightarrow H^+ + {\bullet}OH \quad (15)$$

$$h_{vb}^+ + OH^- \rightarrow {\bullet}OH \quad (16)$$

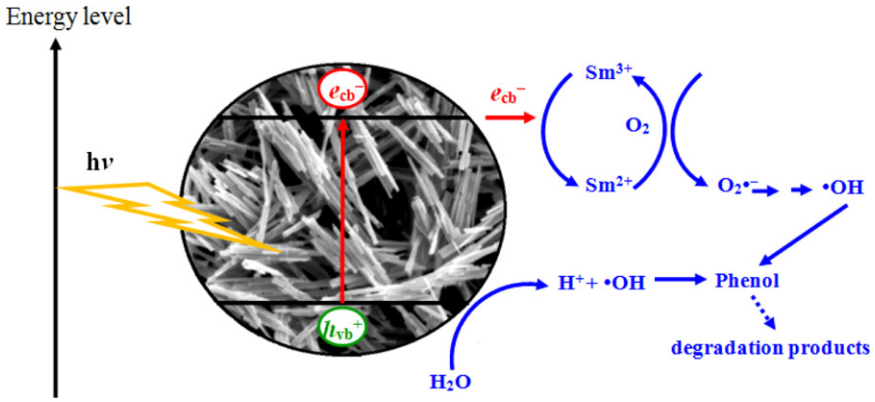

Scheme 2. Possible photocatalytic mechanism of Sm/ZNRs.

Table 2
The comparison of the previously data on the phenol degradation with results finding in the present study.

Photocatalyst	Experimental condition				Degradation rate	Ref.
	[phenol] (mg/L)	Catalyst amount (g/L)	Solution pH	Source of light		
$ZnO/SiO_2/Pt$	100	1.00	7.0	150 W mercury UV lamp	99.9% degradation achieved in 60 min.	[43]
ZnO/MnO_2	20	0.22	6.0	70 W mercury UV-A lamp	About 80–90% degradation obtained 150 min.	[44]
ZnO	75	2.50	5.6	Sunlight	Complete degradation took place in 480 min.	[45]
N-,S- and C-doped ZnO	10 ± 0.5	1.00	6.6	Four 10 W fluorescent light lamps (visible light)	9.9–31.5% degradation achieved in 180 min	[46]
PFT/ZnO	10	1.00	Not available	Three 1 W LED lamp (visible light)	About 40% degradation took place in 120 min	[47]
Na/ZnO, Li/ZnO, K/ZnO	200	1.00	6.5	125 W mercury UV lamp	About 60%, 70% and 80% degradation occurred for K/ZnO, Li/ZnO and Na/ZnO, respectively in 120 min	[48]
Ag/ZnO	20	1.00	Not available	UV-C lamp	Complete degradation obtained in 150 min	[49]
Sm/ZnO	20	2.00	5.2	55 W compact fluorescent lamp (visible light)	95.9% degradation achieved in 300 min	Present study

Thus, the separation of the charge carriers was attributed to such trapping by Sm dopant in ZNRs. Subsequently, enhanced the yield of •OH quantities in the degradation of phenol, which further improved the photocatalytic activity of Sm/ZNRs. Ultimately, Table 2 was prepared to compare the result of the present study with previously reported data on phenol degradation with other ZnO photocatalysts.

4. Conclusions

In the absence of any surfactants, Sm-doped ZnO nanorods (Sm/ZNRs) with different doping contents of Sm were successfully obtained by a facile solvothermal method, and confirmed by XRD, FESEM, EDX, TEM, HRTEM, UV–vis DRS and PL measurements. The proposed method was rather simple, mild, cost-effective and particularly suited for industrial production of Sm/ZNRs. The investigation of photocatalytic ability showed that Sm/ZNRs were differently affected by Sm doping content in the catalyst, Sm/ZNRs amount, initial substrate concentration and solution pH. The Sm/ZNRs prepared at 1 at% showed the highest photocatalytic activity with k_{obs} of $0.0043\ min^{-1}$ under visible light irradiation, and exceeded that of the pure ZNRs by a factor of almost two times. Such enhancement was attributed to the high charge separation efficiency and •OH generation ability as evidenced by the PL spectra. Furthermore, the as-synthesized Sm/ZNRs could be easily recycled without any significant loss of the photocatalytic activity, which was favorable for the potential practical applications.

Acknowledgments

This research was supported by a Research Universiti grant (no. 814176) and a Post Graduate Research Scheme (no. 8045032) from Universiti Sains Malaysia as well as a My PhD scholarship through Malaysia Government.

References

[1] M.P. Lu, J.H. Song, M.Y. Lu, M.T. Chen, Y.F. Gao, L.J. Chen, Z.L. Wang, Piezoelectric nanogenerator using p-type ZnO nanowire arrays, Nano Letters 9 (2009) 1223–1227.
[2] J.A. Anta, E. Guillén, R. Tena-Zaera, ZnO based dye-sensitized solar cells, Journal of Physical Chemistry C 116 (2012) 11413–11425.
[3] S.M. Lam, J.C. Sin, A.Z. Abdullah, A.R. Mohamed, Degradation of wastewaters containing organic dyes photocatalysed by zinc oxide: a review, Desalination and Water Treatment 41 (2012) 131–169.
[4] P. Tonto, O. Mekasuwandumrong, S. Phatanasri, V. Pavarajarn, P. Praserthdam, Preparation of ZnO nanorod by solvothermal reaction of zinc acetate in various alcohols, Ceramics International 34 (2008) 57–62.
[5] G. Meng, X.D. Fang, W.W. Dong, R.H. Tao, Y.P. Zhao, Z.H. Deng, S. Zhou, J.Z. Shao, L. Li, One step synthesis of vertically aligned ZnO nanowire arrays with tunable length, Applied Surface Science 256 (2010) 6543–6549.
[6] Y.C. Liang, Microstructure and optical properties of electrodeposited Al-doped ZnO nanosheets, Ceramics International 38 (2012) 119–124.
[7] P. Mishra, R.S. Yadav, A.C. Pandey, Growth mechanism and photoluminescence property of flower-like ZnO nanostructures synthesized by starch-assisted sonochemical method, Ultrasonics Sonochemistry 17 (2010) 560–565.
[8] D.B. Wang, Y.H. Zhao, C.X. Song, Synthesis and properties of cuboid-shaped ZnO hierarchical structures, Solid State Sciences 12 (2010) 776–782.
[9] B.X. Li, Y.F. Wang, Facile synthesis and enhanced photocatalytic performance of flower-like ZnO hierarchical microstructures, Journal of Physical Chemistry C 114 (2010) 890–896.
[10] R. Yousefi, M.R. Muhamad, A.K. Zak, The effect of source temperature on morphological and optical properties of ZnO nanowires grown using a modified thermal evaporation set-up, Current Applied Physics 11 (2011) 767–770.
[11] S. Ilican, Y. Caglar, M. Caglar, F. Yakuphanoglu, Structural, optical and electrical properties of F-doped ZnO nanorod semiconductor thin films deposited by sol-gel process, Applied Surface Science 255 (2008) 2353–2359.

[12] H.M. Yang, J. Ouyang, A.D. Tang, Single step synthesis of high purity CoO nanocrystals, Journal of Physical Chemistry B 111 (2007) 8006–8013.
[13] R. Razali, A.K. Zak, W.H.Abd. Majid, M. Darroudi, Solvothermal synthesis of microsphere ZnO nanostructures in DEA media, Ceramics International 37 (2011) 3657–3663.
[14] S. Sarkar, S. Patra, S.K. Bera, G.K. Paul, R. Ghosh, Water repellent ZnO nanowire arrays synthesized by simple solvothermal technique, Materials Letters 64 (2010) 460–462.
[15] M.S. Mohajerani, A. Lak, A. Simchi, Effect of morphology on the solar photocatalytic behavior of ZnO nanostructures, Journal of Alloys and Compounds 485 (2009) 616–620.
[16] S.M. Lam, J.C. Sin, A.Z. Abdullah, A.R. Mohamed ZnO nanorods surface-decorated by WO_3 nanoparticles for photocatalytic degradation of endocrine disruptors under a compact fluorescent lamp, Ceramics International. http://dx.doi.org/10.1016/j.ceramint.2012.08.085, in press.
[17] W. Xie, Y.Z. Li, W. Sun, J.C. Huang, H. Xie, X.J. Zhao, Surface modification of ZnO with Ag improves its photocatalytic efficiency and photostability, Journal of Photochemistry and Photobiology A: Chemistry 216 (2010) 149–155.
[18] O. Yayapao, T. Thongtem, A. Phuruangrat, S. Thongtem, Ultrasonic-assisted synthesis of Nd-doped ZnO for photocatalysis, Materials Letters 90 (2013) 83–86.
[19] C. Karunakaran, P. Gomathisankar, G. Manikandan, Preparation and characterization of antimicrobial Ce-doped ZnO nanoparticles for photocatalytic detoxification of cyanide, Materials Chemistry and Physics 123 (2010) 585–594.
[20] J.C. Sin, S.M. Lam, A.R. Mohamed, Optimizing photocatalytic degradation of phenol by TiO_2/GAC using response surface methodology, Korean Journal of Chemical Engineering 28 (2011) 84–92.
[21] J.G. Yu, G.P. Dai, B.B. Huang, Fabrication and characterization of visible-light-driven plasmonic photocatalyst Ag/AgCl/TiO_2 nanotube arrays, Journal of Physical Chemistry C 113 (2009) 16394–16401.
[22] S. Anandan, A. Vinu, T. Mori, N. Gokulakrishnan, P. Srinivasu, V. Murugesan, K. Ariga, Photocatalytic degradation of 2,4,6-trichlorophenol using lanthanum doped ZnO in aqueous suspension, Catalysis Communications 8 (2007) 1377–1382.
[23] Y. Zhou, S.X. Lu, W.G. Xu, Photocatalytic activity of Nd-doped ZnO for the degradation of C.I. Reactive Blue 4 in aqueous suspension, Environmental Progress & Sustainable Energy 28 (2009) 226–233.
[24] R. John, R. Rajakumari, Synthesis and characterization of rare earth ion doped nano ZnO, Nano-Micro Letters 4 (2012) 65–72.
[25] V. Štengl, S. Bakardjieva, N. Murafa, Preparation and photocatalytic activity of rare earth doped TiO_2 nanoparticles, Materials Chemistry and Physics 114 (2009) 217–226.
[26] P.X. Gao, Z.L. Wang, Substrate atomic-termination-induced anisotropic growth of ZnO nanowires/nanorods by the VLS process, Journal of Physical Chemistry B 108 (2004) 7534–7537.
[27] R.A. Laudise, A.A. Ballman, Hydrothermal synthesis of zinc oxide and zinc sulfide, Journal of Physical Chemistry 64 (1960) 688–691.
[28] S.M. Lam, J.C. Sin, A.R. Mohamed, Parameter effect on photocatalytic degradation of phenol using TiO_2-P25/activated carbon (AC), Korean Journal of Chemical Engineering 27 (2010) 1109–1116.
[29] J.K. Fawell, S. Hunt, Environmental Toxicology: Organic Pollutants, Ellis Horwood Limited, Chichester, 1988.
[30] P. Górska, A. Zaleska, J. Hupka, Photodegradation of phenol by UV/TiO_2 and Vis/N,C-TiO_2 processes: comparative mechanistic and kinetic studies, Separation and Purification Technology 68 (2009) 90–96.
[31] A. Sobczyński, Ł. Duczmal, W. Zmudziński, Phenol destruction by photocatalysis on TiO_2: an attempt to solve the reaction mechanism, Journal of Molecular Catalysis A: Chemical 213 (2004) 225–230.
[32] Z.F. Guo, R.X. Ma, G.J. Li, Degradation of phenol by nanomaterial TiO_2 in wastewater, Chemical Engineering Journal 119 (2006) 55–59.
[33] J. Villaseñor, P. Reyes, G. Pecchi, Catalytic and photocatalytic ozonation of phenol on MnO_2 supported catalysts, Catalysis Today 76 (2002) 121–131.
[34] J.C. Sin, S.M. Lam, A.R. Mohamed, K.T. Lee, Degrading endocrine disrupting chemicals from wastewater by TiO_2 photocatalysis: a review, International Journal of Photoenergy 2012 (2012) 1–23.
[35] D.W. Chen, A.K. Ray, Photodegradation kinetics of 4-nitrophenol in TiO_2 suspension, Water Research 32 (1998) 3223–3234.
[36] S. Bekkouche, M. Bouhelassa, N. Hadj Salah, F.Z. Meghlaoui, Study of adsorption of phenol on titanium oxide (TiO_2), Desalination 166 (2004) 355–362.
[37] M. Nasr-Esfahani, A. Khakifirooz, N. Tavakoli, M.H. Soleimani, Preparation, characterization and photocatalytic activity of a novel nanostructure ZnO composite film derived sol-gel process using organic binder materials, Desalination and Water Treatment 21 (2010) 202–209.
[38] C. Sirtori, P.K. Altvater, A.M. de Freitas, G. Peralta-Zamora, Degradation of aqueous solutions of camphor by heterogeneous photocatalysis, Journal of Hazardous Materials B129 (2006) 110–115.
[39] N. Daneshvar, S. Aber, M.S. Seyed Dorraji, A.R. Khataee, M.H. Rasoulifard, Photocatalytic degradation of the insecticide diazinon in the presence of prepared nanocrystalline ZnO powders under irradiation of UV-C light, Separation and Purification Technology 58 (2007) 91–98.
[40] H.J. Liu, G.G. Liu, Q.X. Zhou, G.H. Xie, Z.H. Hou, M.L. Zhang, Z.W. He, Preparation and photocatalytic activity of Gd^{3+}-doped trititanate nanotubes, Microporous and Mesoporous Materials 142 (2011) 439–443.
[41] Y.V. Pleskov, Conversion of luminous energy into electrical and chemical energy in photoelectrochemical cells with semiconductor electrodes (review), Soviet Electrochemistry 17 (1981) 1–25.
[42] A.D. Paola, M. Bellardita, G. Marcì, L. Palmisano, F. Parrino, R. Amadelli, Preparation of Sm-loaded brookite TiO_2 photocatalysts, Catalysis Today 161 (2011) 35–40.
[43] R.M. Mohamed, M.A. Barakat, Enhancement of photocatalytic activity of ZnO/SiO_2 by nanosized Pt for photocatalytic degradation of phenol in wastewater, International Journal of Photoenergy 2012 (2012) 1–8.
[44] S.J. Li, Z.C. Ma, J. Zhang, Y.S. Wu, Y.M. Gong, A comparative study of photocatalytic degradation of phenol of TiO_2 and ZnO in the presence of manganese dioxides, Catalysis Today 139 (2008) 109–112.
[45] S.K. Pardeshi, A.B. Patil, A simple route for photocatalytic degradation of phenol in aqueous zinc oxide suspension using solar energy, Solar Energy 82 (2008) 700–705.
[46] L.C. Chen, Y.J. Tu, Y.S. Wang, R.S. Kan, C.M. Huang, Characterization and photoreactivity of N-, S-, and C-doped ZnO under UV and visible light illumination, Journal of Photochemistry and Photobiology A: Chemistry 199 (2008) 170–178.
[47] R.L. Qiu, D.D. Zhang, Y.Q. Mo, L. Song, E. Brewer, X.F. Huang, Y. Xiong, Photocatalytic activity of polymer-modified ZnO under visible light irradiation, Journal of Hazardous Materials 156 (2008) 80–85.
[48] H. Benhebal, M. Chaib, A. Leonard, S.D. Lambert, M. Crine, Photodegradation of phenol and benzoic acid by sol–gel-synthesized alkali metal-doped ZnO, Materials Science in Semiconductor Processing 15 (2012) 264–269.
[49] R.H. Wang, J.H.Z. Xin, Y. Yang, H.F. Liu, L.M. Xu, J.H. Hu, The characteristics and photocatalytic activities of silver doped ZnO nanocrystallites, Applied Surface Science 227 (2004) 312–317.